

## Article

# Oblique Detonation Wave Control with O<sub>3</sub> and H<sub>2</sub>O<sub>2</sub> Sensitization in Hypersonic Flow

Ashish Vashishtha <sup>1,\*</sup>, Snehasish Panigrahy <sup>2</sup>, Dino Campi <sup>1</sup>, Dean Callaghan <sup>3</sup>, Cathal Nolan <sup>1</sup> and Ralf Deiterding <sup>4</sup>

<sup>1</sup> Department of Aerospace & Mechanical Engineering, South East Technological University (SETU), Carlow Campus, R93 V960 Carlow, Ireland; c00237071@itcarlow.ie (D.C.); cathal.nolan@setu.ie (C.N.)

<sup>2</sup> Department of Energy Science and Engineering, Indian Institute of Technology, Delhi 110016, India; snehasish.panigrahy@dese.iitd.ac.in

<sup>3</sup> The Center for Research and Enterprise in Engineering (engCORE), South East Technological University (SETU), Carlow Campus, R93 V960 Carlow, Ireland; dean.callaghan@setu.ie

<sup>4</sup> Aerodynamics and Flight Mechanics Research Group, University of Southampton, Boldrewood Innovation Campus, Southampton SO16 7QE, UK; r.deiterding@soton.ac.uk

\* Correspondence: ashish.vashishtha@setu.ie



**Citation:** Vashishtha, A.; Panigrahy, S.; Campi, D.; Callaghan, D.; Nolan, C.; Deiterding, R. Oblique Detonation Wave Control with O<sub>3</sub> and H<sub>2</sub>O<sub>2</sub> Sensitization in Hypersonic Flow. *Energies* **2022**, *15*, 4140. <https://doi.org/10.3390/en15114140>

Academic Editor: Andrey Starikovskiy

Received: 6 May 2022

Accepted: 1 June 2022

Published: 4 June 2022

**Publisher's Note:** MDPI stays neutral with regard to jurisdictional claims in published maps and institutional affiliations.



**Copyright:** © 2022 by the authors. Licensee MDPI, Basel, Switzerland. This article is an open access article distributed under the terms and conditions of the Creative Commons Attribution (CC BY) license (<https://creativecommons.org/licenses/by/4.0/>).

**Abstract:** This numerical study investigates the effects of adding a small amount of ignition promoters for controlling the wedge-induced oblique shock wave (OSW) to oblique detonation wave (ODW) transition in a premixed hydrogen–air mixture at hypersonic speeds. The time-dependent two-dimensional compressible Euler equations for multiple thermally perfect species with a reactive source term are solved using adaptive mesh refinement and detailed chemical kinetics. The wedge with a fixed angle of 26° exhibits abrupt to smooth transitions for freestream Mach numbers 7–9 (speeds 2.8–3.2 km/s) at a pressure of 20 kPa and a temperature of 300 K. The small amount (1000 PPM by vol.) of H<sub>2</sub>O<sub>2</sub> and O<sub>3</sub> is found to be effective at significantly reducing the initiation length for the oblique detonation transition for all Mach numbers, which suggests a practical approach to increase the operating flight range for oblique detonation wave engine with a finite length wedge. At Mach number 8, the abrupt OSW to ODW transition turns towards a smooth transition with a small amount of H<sub>2</sub>O<sub>2</sub> and O<sub>3</sub> addition. Comparatively, O<sub>3</sub> addition was found to be effective in reducing the ODW initiation length by promoting reactivity behind even a weaker oblique shock at low Mach number 7, for abrupt transition, while H<sub>2</sub>O<sub>2</sub> addition was more effective than O<sub>3</sub> at high Mach numbers 8 and 9, during a smooth transition. The maximum 73% and 80% reduction in initiation length of ODW was observed with 10,000 PPM H<sub>2</sub>O<sub>2</sub> and O<sub>3</sub> addition, respectively, during an abrupt OSW to ODW transition at Mach 7.

**Keywords:** schramjet; oblique detonation wave; hypersonic flow; detailed chemical kinetics; fuel-sensitization

## 1. Introduction

Between two combustion modes: deflagration and detonation [1], detonation-based combustion systems have been found to achieve a higher heat release rate as well as higher thermodynamic efficiency than the deflagration-based systems. Other advantages, such as simpler design and shorter combustor length, makes a detonation-based combustor system an ideal candidate for integration with future hypersonic transport vehicles. In recent decades, Kailasanath [2] and Wolanski [3] have reviewed the progress of detonation-based propulsion systems, mainly pulse detonation engine (PDE), rotatory detonation engine (RDE) and oblique detonation wave engine (ODWE), also referred to as shock-induced combustion ramjet (or shramjet). Among these three detonation-based propulsive systems, the Oblique detonation wave engine (ODWE) concept has the simplest design and can be easily integrated into a scramjet engine configuration. It requires a wedge in the supersonic

premixed stream of the fuel–air mixture, which can establish a compression wave as an oblique shock wave. Sufficient compression provided by oblique shock can ignite the fuel–air mixture and may turn it into a standing or propagating detonation wave [4], which can be further accelerated through the nozzle. The main challenge in realizing ODWE is to initiate a detonation at a desired location on the finite wedge and stabilize it for a range of flight Mach numbers. In preliminary studies, reactive Rankine–Hugoniot analysis [5,6] is used by approximating ODW as an oblique shock wave (OSW) coupled with an instantaneous heat release to understand the stable oblique detonation wave formation.

In order to obtain a stable oblique detonation wave for a given Mach number and premixed mixture, the deflection angle should be in the range of ( $\theta_{CJ} < \theta < \theta_{detach}$ ), corresponding to weak overdriven ODW. When the high-speed (supersonic or hypersonic) premixed fuel–air mixture (at a given freestream pressure  $P_\infty$  and temperature  $T_\infty$ ) encounters the flow deflection due to the wedge, the oblique shock forms at the tip of the wedge. The oblique shock compresses the fuel–air mixture, and at appropriate compression (combination of  $\theta$  with  $\theta_{CJ} < \theta < \theta_{detach}$  and  $M_\infty$ ), the oblique shock will transit into an oblique detonation wave through two mechanisms: abrupt transition and smooth transition [7]. The abrupt transition consists of oblique shock with a non-reactive initiation zone, deflagration wave and an oblique detonation wave forming a triple point [4,8,9]. In contrast, a smooth transition occurs with a curved shock at high Mach numbers with a requirement of a low activation energy condition. Figueira et al. [10] have proposed that the criteria depend on the ratio of induction time ( $\tau_i$ ) and total reaction time ( $\tau_r$ ) to distinguish between abrupt and smooth transitions and suggested that abrupt transitions occur when  $\tau_i/\tau_r \rightarrow 1$ , whereas smooth transitions occur when  $\tau_i/\tau_r \rightarrow 0$ . Teng et al. [11] have observed various shock patterns at the end of the initiation zone, such as  $\lambda$ , X and Y-shaped shock waves, all through the abrupt transition. Zhang et al. [12] have observed changes in abrupt and smooth transitions by changing the deflection angle numerically. Teng et al. [13] have found that the initiation length and structure are highly dependent on the freestream Mach number and less dependent on pressure. Gao et al. [14] have found that Argon dilution of more than 70% will lead to an abrupt to smooth transition for H<sub>2</sub>–Air mixture at a given wedge angle and hypersonic Mach number. From the above discussion, it is understood that the OSW to ODW transition through abrupt or smooth mechanisms can be controlled with three controlling parameters: inflow Mach number, wedge angle and chemical kinetics.

For practical purposes, it may be required to adjust the deflection angle for a finite length of the wedge in order to achieve a stable oblique detonation wave within its length for its given flight Mach number. Miao et al. [15] suggested that smooth transition provides stable and disturbance resistivity for ODW rather than an abrupt transition pattern. It is also desirable to achieve the transition near the starting point of the wedge to achieve reduced passage height for integration of ODWE. The current study proposes to manipulate the OSW to ODW transition by altering the chemical kinetics for an H<sub>2</sub>–Air premixed fuel–air mixture by adding ignition promoters, such as H<sub>2</sub>O<sub>2</sub> and O<sub>3</sub>, in order to control the oblique detonation wave formation of a finite length wedge. Magzamov et al. [16] have shown that a small amount of these additives can reduce the induction zone length significantly through ZND-calculations due to the production of O atom and OH radicals, respectively. Recently, Crane et al. [17], through experimental studies with O<sub>3</sub> addition, and Kumar et al. [18], through ZND calculations for H<sub>2</sub>O<sub>2</sub> and O<sub>3</sub>, have suggested that using a moderate amount of these ignition promoters can alter only the chemical kinetic effect without changing the gases' dynamic effects. The effectiveness of both ignition promoters, H<sub>2</sub>O<sub>2</sub> and O<sub>3</sub>, has been well understood in fundamental gaseous detonation phenomenon using theoretical and experimental studies. The applications and effects of these ignition promoters on a detonation-based propulsion system have never been studied to the author's knowledge based on a review of the literature. Previous studies related to the oblique detonation wave have researched the effect of inert gas dilutions [14,19,20]. The novelty and motivation of

this current study are to utilize these ignition promoters for an oblique detonation wave system to increase the ODWE operable flight Mach number range for a finite length wedge.

In the previous literature, the experimental studies for ODW formation are mainly performed by shooting a hypervelocity projectile into a premixed combustible mixture [8,21], which can only provide an instantaneous detonation wave structure. Using the wedge in a shock tube facility [4,22] will provide another experimental option, but upstream propagation of the detonation wave through the boundary layer poses an issue of unstart [23] at various in-flow parameters and mixture conditions in the confined channel. Hence, many numerical studies have been performed in the past decade to understand the formation and transition of ODW and the operating range for stable ODW. Li et al. [24] obtained stable ODW with a non-reactive oblique shock wave (initiation zone), deflagration waves, triple point and oblique detonation using numerical simulations, which was confirmed by experimental studies by Viguer et al. [4]. These have been considered standard features for many numerical studies. The previous numerical studies [10,25,26] show that the viscosity and boundary layer have a negligible effect on the oblique detonation transition structures. Therefore, this study uses two-dimensional inviscid numerical simulation to stabilize the (finite length) wedge-induced oblique detonation wave in a premixed H<sub>2</sub>-Air mixture with an equivalence ratio of 1, using detailed chemical kinetics. The abrupt and smooth transition patterns are obtained by varying the hypersonic inflow Mach number. Furthermore, a moderate amount of H<sub>2</sub>O<sub>2</sub> and O<sub>3</sub> were added individually to investigate their effect on the oblique shock to detonation wave transition patterns. The overall objectives of the study are to: (1) numerically investigate the efficacy of ignition promoters H<sub>2</sub>O<sub>2</sub> and O<sub>3</sub> for the control of oblique detonation wave patterns and the formation of a finite length wedge, and (2) understand the mechanism of control by quantifying the amount of additives with respect to change in the initiation length of ODW formation.

## 2. Numerical Method

In this study, the Adaptive Mesh Refinement Object-oriented C++ (AMROC) [27–29] based on the Structured Adaptive Mesh Refinement (SAMR) solver was used with a detailed reaction model, which has been efficiently used for various shock-induced combustion studies and detonation-based simulation problems [15,30,31]. In various numerical studies, AMROC has been successfully used for ODW simulations with a two-step mechanism [32–34], as well as detailed chemical kinetics [15]. In the current study, the simulations are performed by solving two-dimensional time-dependent compressible reactive multi-species Euler equations with detailed chemical kinetics for various incoming flows. The equations and formulations are shown below [27,31]:

$$\frac{\partial \mathbf{U}}{\partial t} + \frac{\partial \mathbf{F}}{\partial x} + \frac{\partial \mathbf{G}}{\partial y} = \mathbf{S} \quad (1)$$

where conservative state vector  $\mathbf{U}$ , flux vectors  $\mathbf{F}$ ,  $\mathbf{G}$  and  $\mathbf{Z}$  and source term  $\mathbf{S}$  are defined below:

$$\mathbf{U} = \begin{Bmatrix} \rho_1 \\ \vdots \\ \rho_n \\ \rho u \\ \rho v \\ e \end{Bmatrix}, \quad \mathbf{F} = \begin{Bmatrix} \rho_1 u \\ \vdots \\ \rho_n u \\ \rho u^2 + p \\ \rho u v \\ u(e + p) \end{Bmatrix},$$

$$\mathbf{G} = \begin{Bmatrix} \rho_1 v \\ \vdots \\ \rho_n v \\ \rho v^2 + p \\ \rho u v \\ v(e + p) \end{Bmatrix}, \quad \mathbf{S} = \begin{Bmatrix} \omega_1 \\ \vdots \\ \omega_n \\ 0 \\ 0 \\ 0 \end{Bmatrix} \quad (2)$$

Total Density:

$$\rho = \sum_{i=1}^n \rho_i \quad (3)$$

Energy:

$$e = \rho h - p + \frac{1}{2} \rho (u^2 + v^2) \quad (4)$$

Specific Enthalpy:

$$h = \sum_{i=1}^n \frac{\rho_i h_i}{\rho} \quad (5)$$

Equation of State:

$$p = \sum_{i=1}^n \rho_i \frac{R}{w_i} T \quad (6)$$

in which the source term  $\omega_i$  is the specific mass production rate of each species, which depends on the forward and backward reaction rates from the detailed chemical reaction mechanism used.  $w_i$  is the molecular weight of each species,  $R$  is the universal gas constant and  $T$  is the local temperature. The hydrogen–air combustion, as well as the H<sub>2</sub>O<sub>2</sub> addition calculations, uses 12 species for 34 reaction-detailed chemical kinetic mechanisms for hydrogen–air detonation, which was derived from Westbrook et al. [35]. However, simulations involving O<sub>3</sub> addition have been modeled by adding Princeton’s Ozone submodel [36] to the Westbrook H<sub>2</sub>–Air Mechanism with a total of 15 species with 46 reactions. This study uses the chemistry module of the AMROC solver, which assumes the thermodynamic equilibrium temperature to estimate mixture properties and reactive source terms. The thermodynamic non-equilibrium effects (multi-temperature model) at hypersonic speeds are not considered at this stage, which will require a completely different solver (e.g., based on Mutation++) with the integration of dissociation chemistry to be developed [37,38]. Shi et al. [39] suggested that the choice of temperature to estimate the reactive source term in non-equilibrium gaseous detonation can lead to discrepancies in estimating the detonation cell size in propagating detonation. The AMROC solver decouples the hydrodynamic transport and chemical reactions numerically by utilizing a time-operator splitting approach or method of fractional steps [28]. In the current solver, Godunov splitting is adopted for decoupling and the second-order accurate MUSCL-TVD finite volume method (FVM) is used for the convective flux discretization. A hybrid Roe-HLL Riemann solver is used for the construction of the inter-cell numerical upwind fluxes, while the min-mod limiter is applied with the MUSCL reconstruction to construct a second-order method in space. The second-order accurate MUSCL-Hancock technique is adopted for time integration. The dynamic time stepping is used for all simulations by using the target CFL number of 0.95, with a minimum time step of  $1 \times 10^{-10}$  s. The structured automatic mesh refinement (SAMR) method based on various flow parameters was utilized here, which has low numerical diffusion in a highly refined region. The details of the computation domain, boundary and initial conditions, solution procedure, as well as the grid independence solution will be discussed in the following subsections.

## 2.1. Computational Domain

The computational domain, with dimensions  $5 \times 6$  cm, is shown in Figure 1, which consists of a wedge with a fixed deflection angle of  $\theta = 26^\circ$ . The wedge tip starts at

$X = 0.0$ , and the inlet and outlet boundaries are kept at  $X = -0.2$  and  $4.8 \text{ cm}$ , respectively. It was expected that the oblique shock wave would be established at the tip of the wedge and transit to an oblique detonation wave at the appropriate distance. The polar curve analysis [5] shows that for a given Mach number and fuel–air mixture if the detonation wave solution exists, it forms a higher angle than the oblique shock wave.

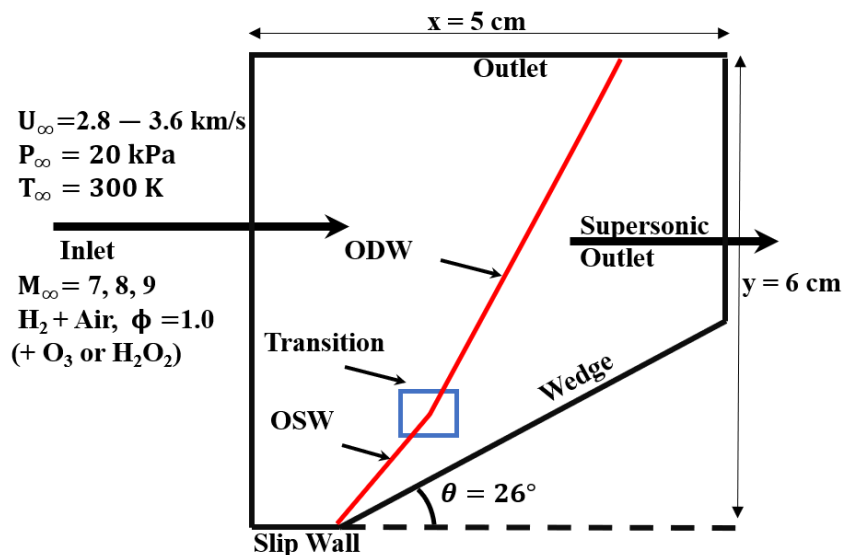


**Figure 1.** Computation domain and boundary conditions.

## 2.2. Boundary and Initial Conditions

Figure 1 also shows the boundary conditions used for all the simulations. The left boundary is used as the inflow boundary condition with appropriate pressure, temperature and inflow speed along with the species assigned, as shown in Table 1. The freestream pressure of  $20 \text{ kPa}$  and a temperature of  $300 \text{ K}$  have been used for all the simulations with a fixed wedge angle of  $26^\circ$ . All the time-dependent simulations were initialized with impulse start and stopped at  $100 \mu\text{s}$ , which was found as a sufficient time interval for the stable oblique shock wave or oblique detonation wave formations. The end solution was analyzed for abrupt and smooth transition patterns, as well as initiation length for the oblique shock to detonation wave transition. The careful choice of Mach number, freestream pressure and temperature conditions results in the selection of a domain (wedge length) to perform the simulation with an adequate grid resolution for the available resources.

**Table 1.** Boundary Condition and Flow Properties.

Description	Value
Freestream Mach Number ( $M_\infty$ )	7, 8, 9
Freestream Speed ( $V_\infty$ )	2.8–3.6 km/s
Freestream Pressure ( $P_\infty$ )	20 kPa
Freestream Temperature ( $T_\infty$ )	300 K
$\text{H}_2\text{-Air}$ Equivalence Ratio ( $\phi$ )	1.0
Deflection Angle ( $\theta$ )	$26.0^\circ$
$M_{CJ}$ (No Additive)	4.75
CJ Speed	1940.09 m/s (No Additive) 1921.37 m/s (10,000 PPM $\text{H}_2\text{O}_2$ ) 1943.28 mm (10,000 PPM $\text{O}_3$ )
CJ-ZND Induction Length	1.04 mm (No Additive) 0.32 mm (10,000 PPM $\text{H}_2\text{O}_2$ ) 0.29 mm (10,000 PPM $\text{O}_3$ )

### 2.3. Grid Independence

To perform the grid independence test, two cases at Mach 7 (with 10,000 PPM H<sub>2</sub>O<sub>2</sub> addition) and Mach 9 (with 10,000 PPM O<sub>3</sub>) have been selected, representing abrupt and smooth transitions of ODW, respectively. At a freestream Pressure of 20 kPa and a temperature of 300 K with a stoichiometric H<sub>2</sub>-Air mixture, the CJ conditions are tabulated in Table 1 with a CJ-ZND induction length of 1.04 mm. The addition of H<sub>2</sub>O<sub>2</sub> and O<sub>3</sub> in the mixture further reduces the CJ-ZND induction length to 0.32 and 0.29 mm, respectively. However, the change in CJ speed is less than 0.01% for the mixture with moderate additives, also tabulated in Table 1. It is recommended to use a high grid resolution of up to 16–64 grid points within the reaction zone for normal detonation simulations. However, Choi et al. [40] and Verreault [41] have obtained grid-independent oblique detonation wave transitions with 5 to 13 grid points, respectively, within the half-reaction length. To obtain adequate grid resolution for abrupt and smooth OSW to ODW transitions, three base grids with four levels of adaptive grid refinements have been considered for both additive cases of Mach 7 and 9. The base grid with uniform sizes of 0.4 (coarse), 0.2 (medium) and 0.1 mm (fine) have been used for all grid independence cases. The same adaptive grid refinement approach was used with four levels: (2, 2, 2, 4), where the minimum grid size was 1/16th of the base grid. The criterion for the adaptive grid resolution used was based on the threshold of pressure and density  $\varepsilon_p = 40,000$ ,  $\varepsilon_\rho = 0.03$ . The mass fraction of the main and intermediate species were also considered for adaptive grid refinement as:  $\varepsilon_{H_2} = 0.012$ ,  $\varepsilon_{O_2} = 0.1$ ,  $\varepsilon_{H_2O} = 0.085$ ,  $\varepsilon_H = 0.002$ ,  $\varepsilon_O = 0.005$  and  $\varepsilon_{OH} = 0.013$ . These threshold conditions remained unchanged for all the base grid simulations.

Figure 2 shows results from the grid independence study performed for freestream Mach 7 for the H<sub>2</sub> and air mixture with a 10,000 PPM H<sub>2</sub>O<sub>2</sub> addition. Figure 2a–c show the variation in pressure, temperature and OH mass fraction along the line parallel to the wedge length (with a 0.2 mm shift). Figure 2d shows the temperature contours for the abrupt transition of the established detonation wave, and Figure 2e shows the used adaptive grid refinement levels (up to 4) in the simulation for a medium grid. The pressure curve in Figure 2a shows the sudden rise in the pressure near the wedge tip, representing the oblique shock wave and the second rise due to ignition and deflagration wave in the compressed region. The next jumps represent the transverse waves in abrupt transition. A similar profile is also seen for temperature variation along the wedge in Figure 2b. The variation in OH mass fraction represents the chemical activity, while pressure and temperature variations represent the gas dynamics structures captured through numerical simulation. All three base grid solutions are able to capture the gas dynamic features of abrupt oblique detonation waves from pressure and temperature curves, as well as chemical activity from the OH mass fraction curve. The coarse grid (base grid 0.4 mm) shows a slight early rise in the deflagration and detonation zones, but medium and fine grids have shown similar initiation structures without significant difference in the gas dynamic and chemical effects. Hence, the medium grid (base grid 0.2 mm) is selected for all of the calculations. The temperature contours are shown in Figure 2d, which clearly captures the oblique shock and abrupt transition through the deflagration zone, triple point, transverse wave, slip line and reflected transverse wave, as well as detonation pattern. Figure 2d shows the four levels of adaptive grid refinement used at time  $t = 100 \mu s$ . The used adaptive refinement criteria based on pressure and density, as well as species, were found to be adequate to capture the main features of ODW abrupt transition. The representation of different levels of refinements is shown in the zoomed image in Figure 2e. The minimum grid size for the medium grid (base grid 0.2 mm) with level 4 adaptive grid refinement is 12.5  $\mu m$ , which represents approximately 25 grid points in the CJ-ZND induction length for 10,000 PPM H<sub>2</sub>O<sub>2</sub> addition. Although, with an overdriven detonation wave at higher Mach numbers, the ZND induction length will be smaller than the CJ-ZND induction length. However, within the scope of the study, all three grid resolutions are able to capture the required detail to estimate the ODW initiation length and pattern adequately. Moreover, another deciding factor for choosing the medium grid solution was computation cost. The single

medium grid solution uses approximately 2800 core hours, while the fine grid solution used approximately 12,000 core hours.

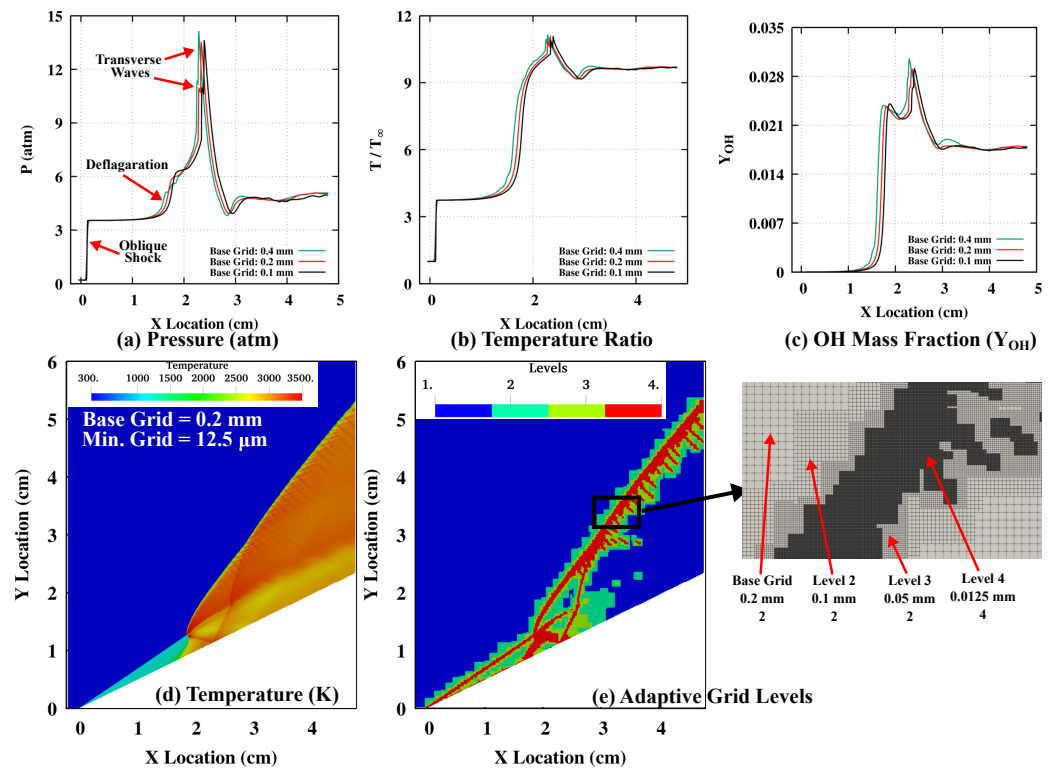


**Figure 2.** Mach 7 with 10,000 PPM  $\text{H}_2\text{O}_2$  addition: (a) Pressure, (b) temperature and (c) OH mass fraction variation at lines parallel to the wedge for all three grids; (d) Temperature and (e) adaptive grid levels for the medium grid.

Further, to validate the grid-independent solution for a smooth transition, the three grid simulations are performed at freestream Mach 9 for the  $\text{H}_2$  and air mixture with 10,000 PPM  $\text{O}_3$  addition, shown in Figure 3. The variation in pressure, temperature and OH mass fraction along the line parallel to the wedge length (with a 0.2 mm shift) are shown in Figure 3a–c. Figure 3d shows the temperature contours for a smooth transition, and Figure 3e shows the adaptive grid refinement levels (up to 4) used in the simulation for a medium grid. All three grids are able to adequately capture the gas dynamics features of a smooth transition as different rises in pressure and temperature curves (Figure 3a,b), representing oblique shock wave, deflagration zone and smooth transition to detonation. Further, all three grids are able to capture the reaction zone, shown as the first peak in OH mass fraction variation (Figure 3c). However, in the post-detonation region, there is a small difference in the OH mass fraction along the wedge. Figure 3c shows the temperature contours for a smooth transition, and Figure 3e shows the level 4 adaptive grid refinements used for a smooth transition. The main objectives of this study are to differentiate between abrupt and smooth transitions of ODW and quantify the effect of  $\text{H}_2\text{O}_2$  and  $\text{O}_3$  addition on the initiation length of the OSW to ODW transition. The grid independence study concludes that it is adequate to use a medium base grid (0.2 mm) and level 4 adaptive grid refinement (minimum grid size 12.5  $\mu\text{m}$ ) for all three freestream Mach numbers 7, 8 and 9, and up to a 10,000 PPM addition of  $\text{H}_2\text{O}_2$  and  $\text{O}_3$ .

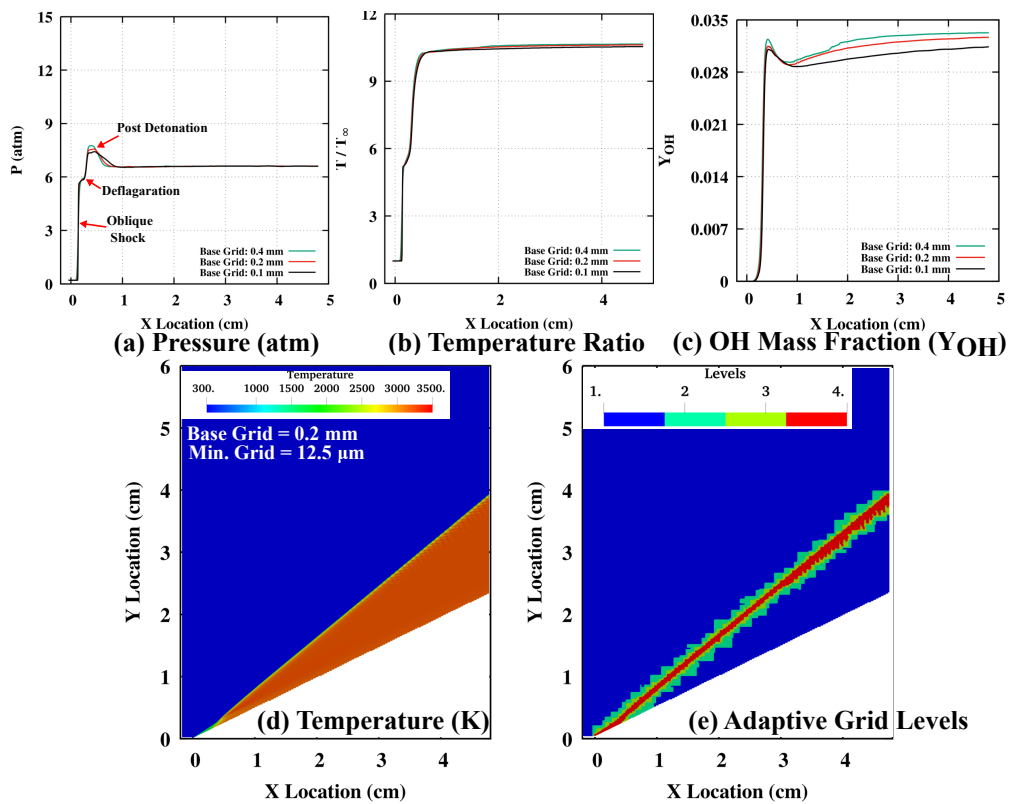


**Figure 3.** Mach 9 with 10,000 PPM O<sub>3</sub> addition: (a) Pressure, (b) temperature and (c) OH mass fraction variation at lines parallel to the wedge for all three grids; (d) Temperature and (e) adaptive grid levels for a medium grid.

### 3. Results and Discussions

The transition pattern of the oblique shock to oblique detonation wave highly depends on the wedge angle, as well as the incoming flow speed and chemical kinetics. It is also well known that low Mach number flow shows abrupt transitions for stoichiometric H<sub>2</sub>-Air premixed mixture when compared to high Mach number flow. To obtain an abrupt to smooth transition for a finite length of wedge, three freestream Mach numbers are selected for an H<sub>2</sub>-Air premixed mixture ( $\phi = 1$ ) at a fixed freestream pressure of 20 kPa and a temperature of 300 K. In further simulations, the incoming H<sub>2</sub>-Air mixture is homogeneously sensitized using H<sub>2</sub>O<sub>2</sub> and O<sub>3</sub> additives in moderate amounts to find their effectiveness for ODW formation. In order to estimate the amount of additive required to control the ODW formation, initially, ZND calculations are performed to estimate the induction length and induction time using the Shock detonation toolbox [42] based on Cantera [43]. Kumar et al. [18] have previously confirmed, using CJ-ZND calculations at 1 atm and 295 K for the H<sub>2</sub>-Air mixture, that the addition of H<sub>2</sub>O<sub>2</sub> and O<sub>3</sub> in moderate amounts can significantly change the ignition chemistry of the unburned mixture without significantly changing its thermodynamic and physical properties. The ignition promotion by H<sub>2</sub>O<sub>2</sub> and O<sub>3</sub> is caused due to reduction in the induction length and induction time because of the shift in the thermic curve towards the shockwave. Figure 4a shows the variation of the induction zone length and induction time for different amounts of H<sub>2</sub>O<sub>2</sub> and O<sub>3</sub> addition. These variations are plotted based on ZND calculations at CJ speeds with the mixture of a pressure of 20 kPa and a temperature of 300 K. The molar concentration of H<sub>2</sub>O<sub>2</sub> and O<sub>3</sub> varied up to 10,000 PPM. The variations in CJ speed are less than 0.01% while varying the amount of additives up to 10,000 PPM does not significantly change the thermodynamic and physical properties of the mixture. The changes in CJ speed with 10,000 PPM additives are mentioned in Table 1. With only 1000 PPM of H<sub>2</sub>O<sub>2</sub> or O<sub>3</sub> addition, the induction length reduces to 50%, and induction time reduces to 57%. However, a further 10-fold increase in concentration can lead to a further 33% reduction in

induction length and induction time. The effect of the Mach number on ZND induction zone length and induction time are also plotted in Figure 4b along with 1000, 5000 and 10,000 PPM  $\text{H}_2\text{O}_2$  or  $\text{O}_3$  addition. The CJ Mach number with no additives is  $M_{CJ} = 4.75$  at 20 kPa and 300 K, which is marked as a straight vertical line in Figure 4b. For all the mixtures, with and without additives, an increase in Mach number from  $M_{CJ}$  to 7 leads to an 85–88% reduction in induction zone length based on ZND calculations and a similar exponential reduction is observed in the induction time. At Mach 9, a ZND solution could not be obtained as the induction length and time become too small. It is noteworthy that the ZND calculation here, which does not represent the wedge-stabilized oblique detonation wave, is a weakly overdriven detonation wave at an angle. The ZND model solves the one-dimensional steady detonation wave, which assumes frozen chemistry across the leading normal shock and postshock of the mixture. The above one-dimensional ZND calculations give an indicative estimate of the amount of additives to influence the induction length and induction time in gaseous detonation. However, the effect of additives on oblique detonation wave structure and its transition characteristics can only be obtained by solving two or three-dimensional equations with detailed chemistry. In the next sections, the results from two-dimensional wedge-stabilized oblique detonation wave simulations are analyzed for three Mach numbers 7, 8 and 9 up to 10,000 PPM  $\text{H}_2\text{O}_2$  as well as  $\text{O}_3$  additives for a finite length wedge. The results are discussed for ODW formation without additives first and then with additives. In order to obtain ODW with a fixed wedge length of 4.8 cm at lower Mach number 7, a minimum addition of 1000 PPM  $\text{H}_2\text{O}_2$  and  $\text{O}_3$  is simulated, along with cases with higher additions of 5000 and 10,000 PPM  $\text{H}_2\text{O}_2$  and  $\text{O}_3$ .

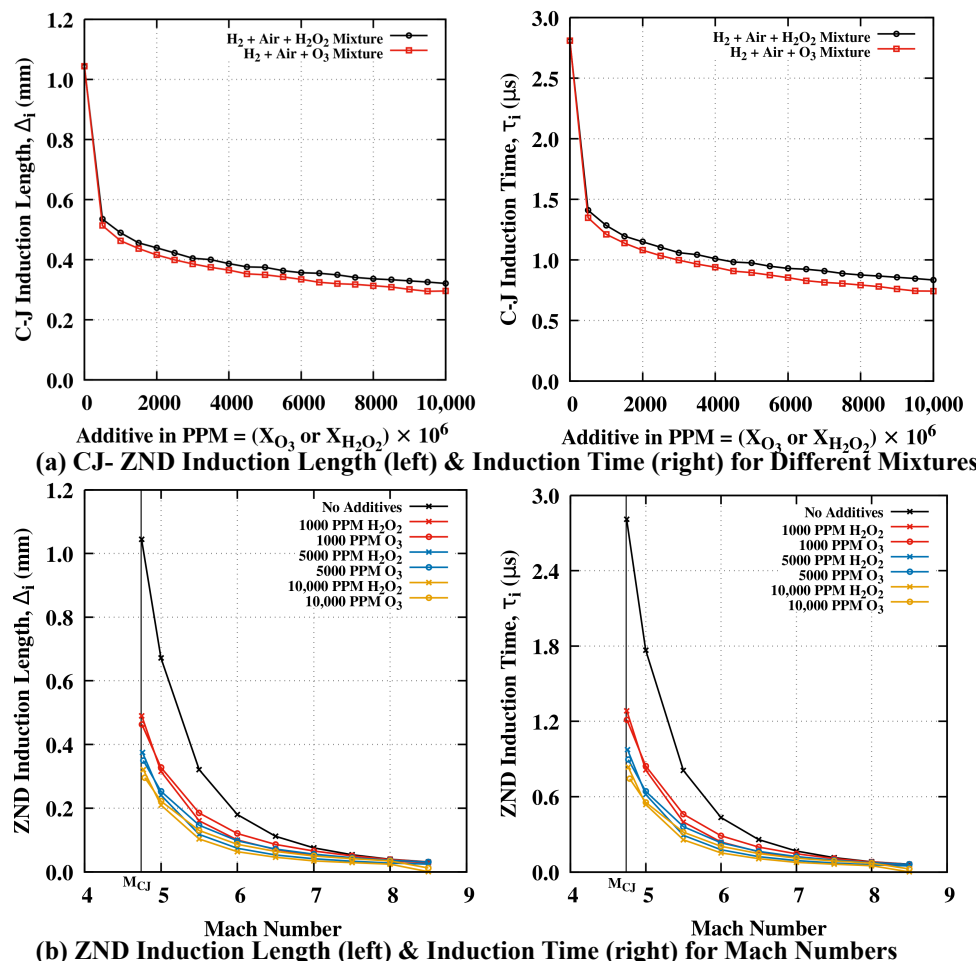


**Figure 4.** Induction Length ( $\Delta_i$ ) and Induction Time ( $\tau_i$ ) variation with (a) Additives, based on CJ-ZND calculation (b) Mach number, based on overdriven ZND calculation.

### 3.1. ODW Formation with No Additives

The inflow Mach number affects the abrupt or smooth transition of OSW to ODW. Hence, the initial simulations for the pure H<sub>2</sub>-Air premixed mixture are performed at three Mach numbers with a fixed wedge angle of 26° and an axial length of 4.8 cm. As the inflow Mach number increases above  $M_{CJ}$  for the given premixed mixture, the minimum deflection angle requirement  $\theta_{CJ}$  rapidly increases [5]. The stoichiometric mixture of H<sub>2</sub>-Air at a pressure of 20 kPa and a temperature of 300 K has the deflection angle window for stable oblique shock between 15.6° and 39.3° at Mach 7. While conducting the initial simulation at Mach 7, the axial length of 4.8 cm for the wedge was not found to be sufficient to establish ODW. Hence, in this particular case at Mach 7, the axial wedge length was increased to 10.8 cm with a domain size of 11 × 10 cm, without changing the adopted grid resolution to obtain the abrupt transition of OSW to ODW, as shown in Figure 5d. All other cases, even with H<sub>2</sub>O<sub>2</sub> and O<sub>3</sub> additives at Mach 7, are simulated with a 4.8 cm axial length wedge size. It can be assumed that there is no ODW formation at Mach 7 for 4.8 cm axial wedge length. However, the wedge length was increased to confirm that the selected finite wedge length was not sufficient to establish an ODW at Mach 7, even when the deflection angle was 10° higher than  $\theta_{CJ}$  at Mach 7. Figure 5a shows the pressure variation along a line parallel to the wedge (with a 0.2 mm shift). Along the line, the first pressure jump occurs near the wedge tip due to non-reactive OSW. The shock-related pressure jump increases with an increase in Mach number due to higher compression. At a further axial distance, the pressure jumps again near the initiation zone of ODW and both the curves at Mach 7 and 8 consist of ripples due to abrupt ODW transition because of the presence of transverse and reflected waves. At Mach 9, OSW to ODW transition occurs due to smooth curved shock, and the pressure curve shows a smooth single peak near the initiation zone. Figure 5b,c shows the OH and O mass fraction along the wedge surface, reflecting the chemical activity near the initiation and flame zones. The two peaks in OH (Figure 5b) and O (Figure 5c) mass fractions correspond to the initial coalesced and downstream transverse waves. With an increase in Mach number, the ODW transition pattern changes from an abrupt to a smooth transition, and the gap between these two peaks decreases or the second peak becomes a plateau due to the non-existence (or weakening) of transverse waves in a smooth transition.

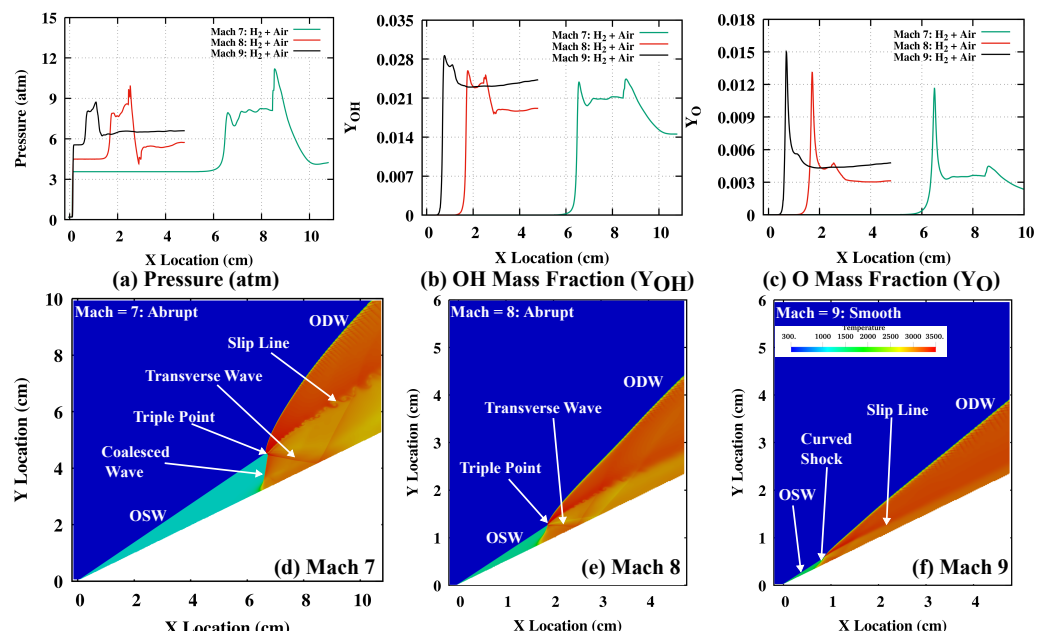


**Figure 5.** (a) Pressure, (b) OH Mass Fraction and (c) O Mass Fraction variation along the wedge surface and temperature contours for (d) Machs 7, (e) 8 and (f) 9 freestream flows without additives.

Various flow features are mentioned for Machs 7 and 8 abrupt transition and Mach 9 smooth transition in Figure 5d–f. At Mach 7 abrupt transition, the triple-point separates OSW and ODW and the front coalesced wave and transverse wave forms a  $\lambda$ -shape shock pattern. An unstable slip line with roll-up behavior of the K-H instability in the detonation zone, along with a reflected transverse wave, is also captured at the abrupt transition. The simulations also show detonation cell-like structures in ODW. Qualitatively, the above numerical simulation result at Mach 7 captures a non-reactive initiation zone, deflagration waves and oblique detonation wave experimentally visualized by Viguier [4]. Recently, Zhang et al. [44] have also reported clear experimental flow features captured from an ODWE model experiment in a hypersonic wind tunnel ( $M_{\infty} = 6.6$ ), with the abrupt transition termed as the strong ODW mode. The oblique detonation wave forms as an oblique Mach stem due to the confined space. These results confirm the presence of a triple point and transverse wave in the experiment, similar to flow features obtained in the above numerical simulation shown in Figure 5d. At Mach 8 (Figure 5e) also, an abrupt transition was observed with a triple point dividing the OSW and ODW and with weaker coalesced and transverse waves (than Mach 7) behind the initiation zone. The angle of ODW has been reduced at the higher Mach number 8 when compared to Mach 7. At Mach 9 (Figure 5f), the triple point has almost disappeared, and a smooth transition occurs with the curved shock and transverse wave disappearing, while the slip line behind the initiation zone becomes parallel to the wedge. The weak detonation result reported by Zhang et al. [44] shows a smooth transition of OSW to ODW with the absence of a triple point and the formation of a series of compression waves transitioning to an oblique detonation wave. Similar flow features are observed in the smooth transition obtained at Mach 9 (in Figure 5f). The oblique detonation wave angle becomes smaller in the weak (smooth transition) ODW mode compared to the strong (abrupt transition) ODW mode from experiments. Table 2 compares the theoretical and numerical ODW angles for the simulated conditions. The theoretical ODW angle is obtained assuming post-shock equilibrium conditions with  $M - \beta - \theta$  relation and a fixed wedge angle ( $\theta = 26^\circ$ ). At Machs 7 and 9, the ODW angles match well with the theoretical values; however, there is a small difference in theoretical and numerical ODW angles at Mach 8. It is evident here that the OSW to ODW transition may occur abruptly at lower Mach numbers for fixed wedge angles and premixed mixtures. However, high Mach numbers show smooth transitions with a smaller initiation length. The initiation length is quantified here from the intermediate O atom peaks along the wedge surface. The axial initiation length at Mach 7 is observed as 6.5 cm (beyond 4.8 cm wedge), and it is estimated as 1.70 and 0.69 cm at Mach 8 and 9, respectively. In the next sections, the effect of chemistry is evaluated on OSW to ODW transition by adding  $H_2O_2$  and  $O_3$  of up to 10,000 PPM in premixed  $H_2$ -Air mixture (at  $\phi = 1$ ).

**Table 2.** Comparison of Theoretical and Numerical ODW Angles (No Additives).

Mach Number	Theoretical ODW Angle	Numerical ODW Angle
Mach = 7	47.7°	47.1°
Mach = 8	42.5°	44.9°
Mach = 9	39.2°	38.9°

### 3.2. Effect of $H_2O_2$ and $O_3$ Addition at Mach 7

The preliminary ZND calculations for CJ speed in Figure 4 show that a small amount, such as 1000 PPM addition of  $H_2O_2$  and  $O_3$ , can significantly reduce the induction zone length and induction time by ignition promotion. On the one hand, ozone can be easily decomposed into  $O_2$  and O atoms at all concentration levels by the third body reaction. The O atom in the induction zone accelerates the chain branching process, which leads to a reduction in the ignition time delay. On the other hand, hydrogen peroxide can be readily decomposed into 2 hydroxyl OH radicals by third body reaction, leading to rapid

temperature rise and reduction in the ignition time delay. At Mach 7, we can assume that a wedge with a finite axial length of 4.8 cm could not establish the ODW (the axial initiation length is 6.5 cm, as shown with the larger domain simulation in the previous Section 3.1). The numerical simulations are performed for 1000, 5000 and 10,000 PPM addition of  $\text{H}_2\text{O}_2$  and  $\text{O}_3$  at this Mach number. In order to understand the chemical effect of additives on ODW formation, the mass fraction of intermediate species, O and OH, are plotted along the wedge axial length in Figure 6b,c. Pressure variation along the wedge (Figure 6a) and temperature (Figure 6d), and pressure contours (Figure 6e) are plotted to understand the gas dynamics effects. With the small amount (1000 PPM) of  $\text{O}_3$  and  $\text{H}_2\text{O}_2$  added, the oblique detonation wave stabilizes on a finite length wedge with a 2.45 cm axial initiation length (62% reduction). Both  $\text{O}_3$  and  $\text{H}_2\text{O}_2$  addition shows similar profiles to O and OH mass fraction variation in Figure 6b,c. However, the OSW to ODW transition remains abrupt in nature with a  $\lambda$ -shock pattern for both additive cases of 1000 PPM  $\text{O}_3$  and  $\text{H}_2\text{O}_2$ , which is clearly reflected as double peaks in pressure, OH and O mass fraction plots, as well as temperature and pressure contours for 1000 PPM  $\text{H}_2\text{O}_2$  addition. The further addition of 5000 and 10,000 PPM additives reduces the initiation length to establish the ODW, but the nature of the transition does not change. The intermediate species mass fraction, as well as pressure curves, show similar profiles but a shift in the axial direction. The higher additions of  $\text{O}_3$  and  $\text{H}_2\text{O}_2$  show a slight difference in their effectiveness. The  $\text{O}_3$  addition further reduces the initiation length in comparison to the same amount of  $\text{H}_2\text{O}_2$  addition. It can be understood that  $\text{O}_3$  decomposition is prevalent even at lower compressed temperature and pressures (in comparison with higher Mach numbers) after the oblique shock at Mach 7, while the OH formation increases at the upstream location on the wedge (2nd peak is higher in the OH profile).  $\text{H}_2\text{O}_2$  may require a higher temperature to decompose into OH. Additionally,  $\text{O}_3$  can also increase the  $\text{O}_2$  concentration near the end of the initiation length, which can significantly promote reactivity in the compressed region.

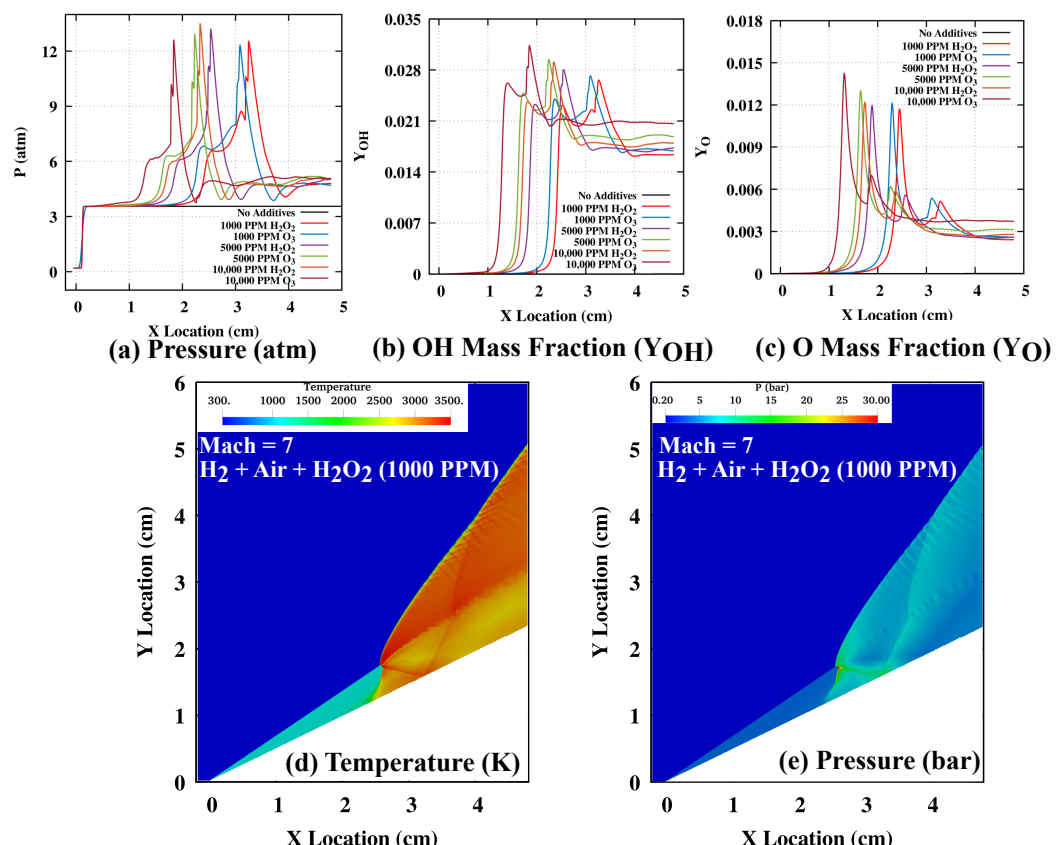


**Figure 6.** (a) Pressure, (b) OH Radical Mass fraction, (c) O variation along the wedge surface, (d) temperature, and (e) pressure contour for 1000 PPM  $\text{H}_2\text{O}_2$  Addition at Mach 7.

### 3.3. Effect of $H_2O_2$ and $O_3$ Addition at Mach 8

The ODW formation at Mach 8 shows features of an abrupt OSW to ODW transition in Figure 5e with a triple-point, transverse wave slip line, reflected transverse wave. However, a steeper detonation wave angle can be observed at Mach 8 when compared to the lower Mach number 7. Figure 7 shows the chemical and gas dynamics effects of 1000, 5000 and 10,000 PPM  $H_2O_2$  and  $O_3$  addition at the Mach 8 ODW transition. A small amount of 1000 PPM can significantly reduce the initiation length on the wedge. It is observed that the addition of 1000 PPM  $H_2O_2$  is more effective in reducing the initiation length than the same amount of  $O_3$ . The pressure variation, which shows ripples after the second jump due to an abrupt shock pattern without any additive, becomes smoother with 1000 PPM  $H_2O_2$  addition, suggesting a change in abrupt to smooth OSW to ODW transition. The mass fraction of intermediate species OH (Figure 7b) and O (Figure 7c) shows two peaks in the no additive case the downstream peak disappears or modifies to a plateau with an increase in additive amounts due to the disappearing or weakening of the transverse wave. The OH mass fraction shows a higher first peak than the second peak (opposite to the Mach 7 case in Figure 6a), suggesting that  $H_2O_2$  decomposition becomes dominant to increase the reactivity after the Mach 8 compressed oblique shock. The OH-dominant ignition promotion rapidly increases the temperature in a smaller zone, which may benefit a smooth transition of the ODW formation. The temperature (Figure 7d) and pressure (Figure 7e) for 5000 PPM  $O_3$  addition show features of a smooth OSW to ODW transition, such as the curved shock, a disappearance of the transverse wave and a slip line parallel to the wedge. Furthermore, a 10,000 PPM addition of  $H_2O_2$  and  $O_3$  leads to OSW to ODW transition closer to the wedge tip with no significant reduction in initiation length as compared to the addition of 1000 PPM. However,  $H_2O_2$  addition is still marginally effective when compared to the same amount of  $O_3$  addition. As the OSW to ODW transition at Mach 8 is moderately abrupt in the case of no additive, the addition of an ignition promoter can change the transition pattern from abrupt to smooth with a rapid increase in temperature and reduction in the initiation length.

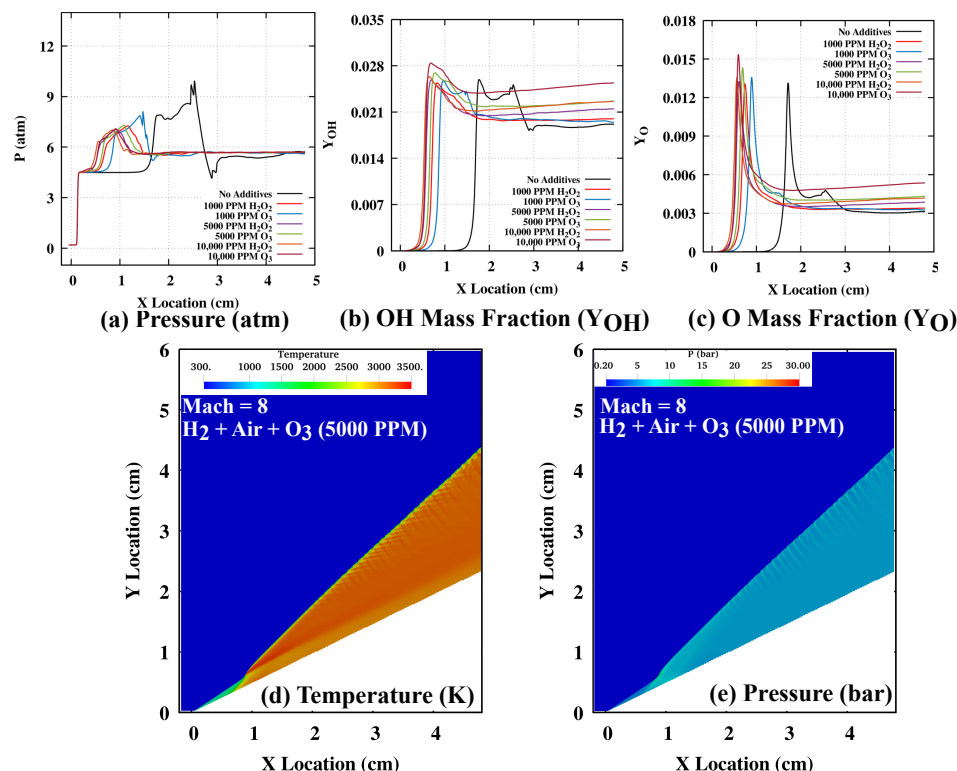


**Figure 7.** (a) Pressure, (b) OH Radical Mass fraction, (c) O variation along the wedge surface, (d) temperature and (e) pressure contour for 5000 PPM  $O_3$  addition at Mach 8.

### 3.4. Effect of $H_2O_2$ and $O_3$ Addition at Mach 9

The OSW to ODW transition at Mach 9 is smooth in nature. Figure 8 shows the variation of pressure and intermediate species, the mass fractions near the wedge surface parallel line, and the temperature, pressure contours for the 1000 PPM  $O_3$  addition. For the no additive case at Mach 9, in Figure 4d, the OSW to ODW smooth transition occurs at the 0.78 cm axial distance, which also shows the curved shock and no triple point formation with the slip line parallel to the wedge. The pressure and intermediate species variation in Figure 7a–c shows a smooth single peak in the reaction zone for the no additive case. The small 1000 PPM addition of  $H_2O_2$  and  $O_3$  additives shifts the reaction zone towards the wedge tip, with the  $H_2O_2$  addition leading to a higher initiation length reduction when compared to the same amount of  $O_3$  addition. As  $H_2O_2$  decomposition occurs at slightly elevated temperatures when compared to  $O_3$  decomposition, the highly compressed region behind the oblique shock at the higher Mach number can provide favorable conditions for  $H_2O_2$  decomposition. A further rapid increase in temperature due to OH formation can facilitate the smooth transition of OSW to ODW formation. The increase in  $H_2O_2$  and  $O_3$  addition to 5000 and 10,000 PPM further reduces the initiation length and moves the transition region closer to the wedge tip. The effectiveness of the  $H_2O_2$  addition is still better for initiation length reduction than the same amount of  $O_3$  addition at higher PPMs. The temperature and pressure contours of 1000 PPM  $O_3$  addition show no significant change in ODW angle when compared to the no additive case (Figure 5f).

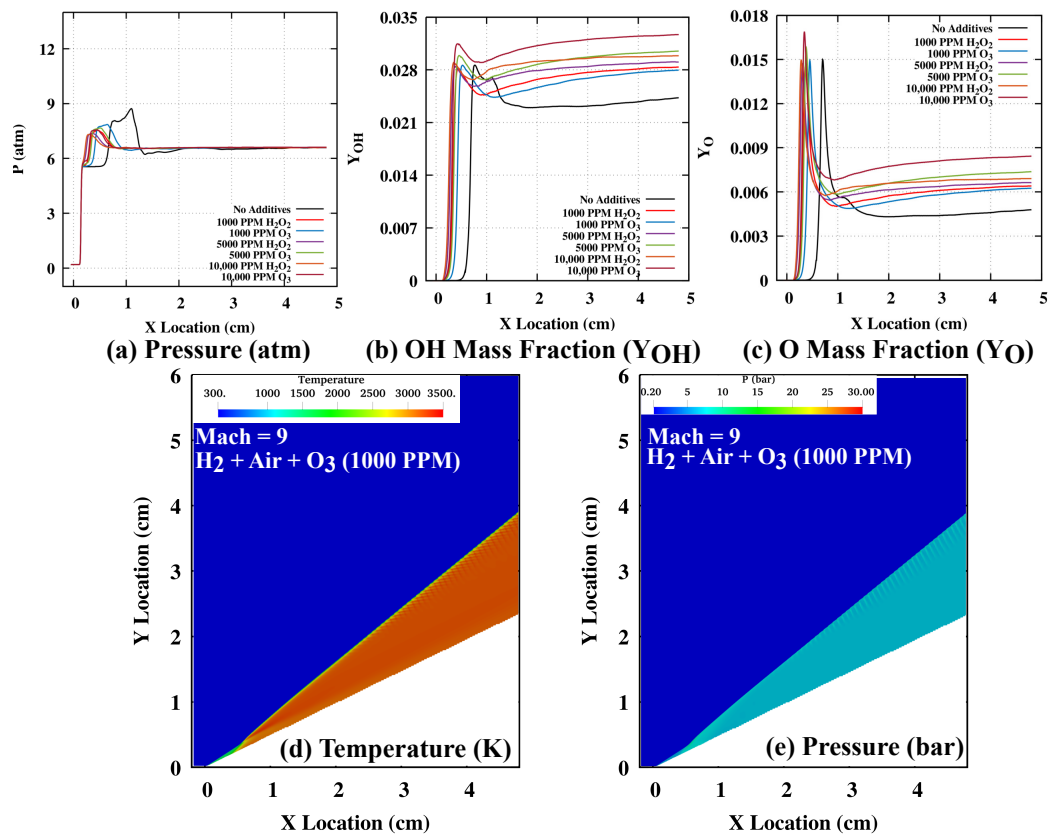


**Figure 8.** (a) Pressure, (b) OH Radical Mass fraction, (c) O variation along the wedge surface, (d) temperature and (e) pressure contour for 1000 PPM  $O_3$  addition at Mach 9.

### 3.5. Effect on ODW Initiation Length

Figure 9a,b quantify the effectiveness of  $H_2O_2$  and  $O_3$  addition on ODW initiation length control. The initiation length ( $L_w$ ) is defined as the length along the wedge surface when the peak oxygen atom (O) mass fraction occurs. The axial X distance is converted to the initiation length with the use of the simulated wedge angle of  $\theta = 26^\circ$ . In the case of

no additives, the initiation lengths computed are 7.2, 1.89 and 0.78 cm for Mach 7, 8 and 9, respectively. In the case of Mach 7, the ODW formation occurs beyond the finite wedge length (of 4.8 cm) used in the current study. As the Mach number increases from 7 to 9, the OSW to ODW transition moves from abrupt to moderately abrupt and to a smooth transition, moving towards the wedge tip. With the increase in Mach number for a fixed wedge angle, the compression by initial OSW in the initiation zone increases the pressure and temperature near the wedge tip, and the oblique shock becomes closer to the wedge surface. With the higher pressure and temperature after the oblique shock, the fuel-air mixture can achieve ignition closer to the wedge tip and leads to an abrupt to a smoother transition. Figure 9b also shows the percentage reduction in initiation length by use of a small and moderate amount of  $\text{H}_2\text{O}_2$  and  $\text{O}_3$  additives. It can be observed that with a small amount of 1000 PPM, the initiation length is significantly reduced at the lower Mach 7 by approximately 62.3%, with a further increase in additive content, an  $\text{O}_3$  addition of 10,000 PPM can lead to a maximum initiation length reduction of 80%, while 10,000 PPM of  $\text{H}_2\text{O}_2$  addition can reduce the initiation length by 73%. At higher Mach numbers, it can be seen that  $\text{H}_2\text{O}_2$  performs well in reducing the initiation lengths in comparison to the same amount of  $\text{O}_3$ . It can be concluded that  $\text{H}_2\text{O}_2$  provides better performance in reducing the initiation length at higher Mach numbers or near the smooth OSW to ODW transition operation, while  $\text{O}_3$  is a very effective ignition promoter in the lower Mach number range, and  $\text{O}_3$  can be helpful for increasing the lower operating flight speed in detonation mode with a very small addition.

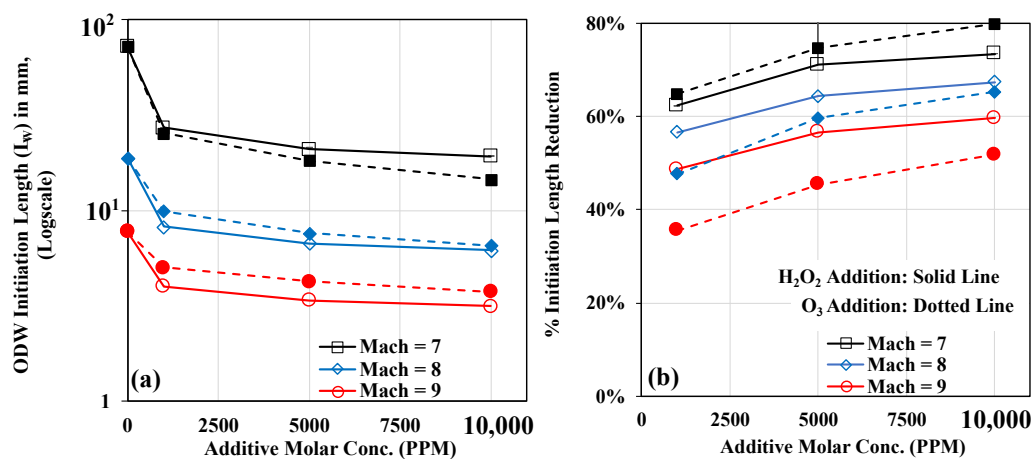


**Figure 9.** Initiation length (a) variation and, (b) percentage reduction with additives at  $\text{H}_2\text{-Air}$  ( $\phi = 1$ ) premixed mixture.

#### 4. Conclusions

The effect of ignition promoters on wedge-induced oblique detonation wave formation was investigated by using two-dimensional compressible reactive flow simulations. The  $\text{H}_2\text{-Air}$  premixed incoming flow with and without  $\text{H}_2\text{O}_2$  and  $\text{O}_3$  addition were simulated at three hypersonic Mach numbers 7, 8 and 9, in front of a finite length wedge. From the obtained results, the following can be concluded:

1. The mixing of  $\text{H}_2\text{O}_2$  and  $\text{O}_3$  from a small amount, 1000 PPM, to a moderate amount, 10,000 PPM, can effectively reduce the initiation lengths of an oblique shock to oblique detonation wave transition at all Mach numbers studied.
2. At Mach 7, the reduction in initiation length is up to 80% with  $\text{H}_2\text{O}_2$  and  $\text{O}_3$  addition during the abrupt transition. The  $\text{O}_3$  addition has been found to be more effective in comparison to the  $\text{H}_2\text{O}_2$  addition for low Mach number abrupt transition conditions, and it can be utilized to increase lower operating flight speeds for ODWE.
3. At Mach 8, the moderate abrupt OSW to ODW transition can be modified to a smoother transition by adding a small amount of  $\text{H}_2\text{O}_2$  and  $\text{O}_3$ . Furthermore,  $\text{H}_2\text{O}_2$

addition has been found to be more effective in reducing the initiation length in comparison to the same amount of O<sub>3</sub> addition for Mach 8 and 9 during smooth ODW transitions.

4. The Mach number dependence of the compressed region in the initiation zone behind the oblique was responsible for the different performances of H<sub>2</sub>O<sub>2</sub> and O<sub>3</sub> addition for initiation length reduction. O<sub>3</sub> decomposition was dominated regarding the initiation length reduction at a relatively lower Mach number, while OH formation from H<sub>2</sub>O<sub>2</sub> was dominant at higher Mach numbers.

**Author Contributions:** Conceptualization: A.V.; methodology and solver: R.D.; mechanism integration, S.P.; simulations: A.V. and D.C. (Dino Campi); formal analysis and investigation, A.V. and S.P.; resources: D.C. (Dean Callaghan) and C.N.; writing—original draft preparation, A.V.; writing—review and editing, A.V., S.P., D.C. (Dean Callaghan), C.N. and R.D. All authors have read and agreed to the published version of the manuscript.

**Funding:** This research received no external funding.

**Institutional Review Board Statement:** Not applicable.

**Informed Consent Statement:** Not applicable.

**Data Availability Statement:** Not applicable.

**Acknowledgments:** The authors would like to acknowledge the Irish Centre for High-End Computing (ICHEC) for the provision of computing resources for this study.

**Conflicts of Interest:** The authors declare no conflict of interest.

## References

1. Lee, J.H.S. *The Detonation Phenomenon*, 1st ed.; Cambridge University Press: Cambridge, UK, 2008. [[CrossRef](#)]
2. Kailasanath, K. Review of Propulsion Applications of Detonation Waves. *AIAA J.* **2000**, *38*, 1698–1708. [[CrossRef](#)]
3. Wolanski, P. Detonative propulsion. *Proc. Combust. Inst.* **2013**, *34*, 125–158. [[CrossRef](#)]
4. Viguier, C.; da Silva, L.F.F.; Desbordes, D.; Deshaies, B. Onset of oblique detonation waves: Comparison between experimental and numerical results for hydrogen-air mixtures. *Symp. (Int.) Combust.* **1996**, *26*, 3023–3031. [[CrossRef](#)]
5. Pratt, D.T.; Humphrey, J.W.; Glenn, D.E. Morphology of standing oblique detonation waves. *J. Propuls. Power* **1991**, *7*, 837–845. [[CrossRef](#)]
6. Powers, J.M.; Stewart, D.S. Approximate solutions for oblique detonations in the hypersonic limit. *AIAA J.* **1992**, *30*, 726–736. [[CrossRef](#)]
7. Wang, A.F.; Zhao, W.; Jiang, Z.L. The criterion of the existence or inexistence of transverse shock wave at wedge supported oblique detonation wave. *Acta Mech. Sin.* **2011**, *27*, 611–619. [[CrossRef](#)]
8. Verreault, J.; Higgins, A.J. Initiation of detonation by conical projectiles. *Proc. Combust. Inst.* **2011**, *33*, 2311–2318. [[CrossRef](#)]
9. Rosato, D.A.; Thornton, M.; Sosa, J.; Bachman, C.; Goodwin, G.B.; Ahmed, K.A. Stabilized detonation for hypersonic propulsion. *Proc. Natl. Acad. Sci. USA* **2021**, *118*, e2102244118. [[CrossRef](#)] [[PubMed](#)]
10. Silva, F.D.; Deshaies, B. Stabilization of an oblique detonation wave by a wedge: A parametric numerical study. *Combust. Flame* **2000**, *121*, 152–166. [[CrossRef](#)]
11. Teng, H.; Zhang, Y.; Jiang, Z. Numerical investigation on the induction zone structure of the oblique detonation waves. *Comput. Fluids* **2014**, *95*, 127–131. [[CrossRef](#)]
12. Zhang, Y.; Yang, P.; Teng, H.; Ng, H.D.; Wen, C. Transition Between Different Initiation Structures of Wedge-Induced Oblique Detonations. *AIAA J.* **2018**, *56*, 4016–4023. [[CrossRef](#)]
13. Teng, H.; Ng, H.D.; Jiang, Z. Initiation characteristics of wedge induced oblique detonation waves in a stoichiometric hydrogen air mixture. *Proc. Combust. Inst.* **2017**, *36*, 2735–2742. [[CrossRef](#)]
14. Gao, Y.; Li, H.; Xiang, G.; Peng, S. Initiation characteristics of oblique detonation waves from a finite wedge under argon dilution. *Chin. J. Aeronaut.* **2021**, *34*, 81–90. [[CrossRef](#)]
15. Miao, S.; Zhou, J.; Lin, Z.; Cai, X.; Liu, S. Numerical Study on Thermodynamic Efficiency and Stability of Oblique Detonation Waves. *AIAA J.* **2018**, *56*, 3112–3122. [[CrossRef](#)]
16. Magzumov, A.E.; Kirillov, I.A.; Rusanov, V.D. Effect of small additives of ozone and hydrogen peroxide on the induction-zone length of hydrogen-air mixtures in a one-dimensional model of a detonation wave. *Combust. Explos. Shock Waves* **1998**, *34*, 338–341. [[CrossRef](#)]
17. Crane, J.; Shi, X.; Singh, A.V.; Tao, Y.; Wang, H. Isolating the effect of induction length on detonation structure: Hydrogen–oxygen detonation promoted by ozone. *Combust. Flame* **2019**, *200*, 44–52. [[CrossRef](#)]

18. Kumar, D.S.; Ivin, K.; Singh, A.V. Sensitizing gaseous detonations for hydrogen/ethylene-air mixtures using ozone and  $H_2O_2$  as dopants for application in rotating detonation engines. *Proc. Combust. Inst.* **2021**, *38*, 3825–3834. [CrossRef]
19. Qin, Q.; Zhang, X. Nitrogen dilution effects on the local detachment of the oblique detonation wave in the  $2H_2-O_2$  mixture. *Int. J. Hydrogen Energy* **2021**, *46*, 6873–6884. [CrossRef]
20. Zhang, Y.; Fang, Y.; Ng, H.D.; Teng, H. Numerical investigation on the initiation of oblique detonation waves in stoichiometric acetylene–oxygen mixtures with high argon dilution. *Combust. Flame* **2019**, *204*, 391–396. [CrossRef]
21. Maeda, S.; Inada, R.; Kasahara, J.; Matsuo, A. Visualization of the non-steady state oblique detonation wave phenomena around hypersonic spherical projectile. *Proc. Combust. Inst.* **2011**, *33*, 2343–2349. [CrossRef]
22. Viguier, C.; Gourara, A.; Desbordes, D. Three-dimensional structure of stabilization of oblique detonation wave in hypersonic flow. *Symp. (Int.) Combust.* **1998**, *27*, 2207–2214. [CrossRef]
23. Sosa, J.; Rosato, D.A.; Goodwin, G.B.; Bachman, C.L.; Oran, E.S.; Ahmed, K.A. Controlled detonation initiation in hypersonic flow. *Proc. Combust. Inst.* **2021**, *38*, 3513–3520. [CrossRef]
24. Li, C.; Kailasanath, K.; Oran, E.S. Detonation structures behind oblique shocks. *Phys. Fluids* **1994**, *6*, 1600–1611. [CrossRef]
25. Li, C.; Kailasanath, K.; Oran, E. Effects of boundary layers on oblique-detonation structures. In Proceedings of the 31st Aerospace Sciences Meeting, Reno, NV, USA, 11–14 January 1993; AIAA: Reston, VI, USA, 1993; Chapter AIAA-93-0450, p. 13. [CrossRef]
26. Oran, E.S.; Weber, J.W.; Stefaniw, E.I.; Lefebvre, M.H.; Anderson, J.D. A Numerical Study of a Two-Dimensional  $H_2-O_2-Ar$  Detonation Using a Detailed Chemical Reaction Model. *Combust. Flame* **1998**, *113*, 147–163. [CrossRef]
27. Deiterding, R. Parallel Adaptive Simulation of Multi-Dimensional Detonation Structures. Ph.D. Thesis, Brandenburgische Technische Universität Cottbus, Cottbus, Germany, 2003.
28. Deiterding, R. High-Resolution Numerical Simulation and Analysis of Mach Reflection Structures in Detonation Waves in Low-Pressure  $H_2-O_2-Ar$  Mixtures: A Summary of Results Obtained with the Adaptive Mesh Refinement Framework AMROC. *J. Combust.* **2011**, *2011*, 738969. [CrossRef]
29. Deiterding, R. A parallel adaptive method for simulating shock-induced combustion with detailed chemical kinetics in complex domains. *Comput. Struct.* **2009**, *87*, 769–783. [CrossRef]
30. Harmon, P.; Vashishtha, A.; Callaghan, D.; Nolan, C.; Deiterding, R., Study of Direct Gas Injection into stagnation zone of Blunt Nose at Hypersonic Flow. In Proceedings of the AIAA Propulsion and Energy 2021 Forum, Virtual, 9–11 August 2021; AIAA: Reston, VI, USA, 2021; Chapter Session, p. 3529. [CrossRef]
31. Vashishtha, A.; Callaghan, D.; Nolan, C.; Deiterding, R. Numerical Investigation of Detonation Propagation Through Small Orifice Holes. *Trans. Aerosp. Res.* **2021**, *2021*, 17–33. [CrossRef]
32. Liu, Y.; Wang, L.; Xiao, B.; Yan, Z.; Wang, C. Hysteresis phenomenon of the oblique detonation wave. *Combust. Flame* **2018**, *192*, 170–179. [CrossRef]
33. Liu, Y.; Xiao, B.; Wang, L.; Wang, C. Numerical Study of Disturbance Resistance of Oblique Detonation Waves. *Int. J. Aerosp. Eng.* **2020**, *2020*. [CrossRef]
34. Huang, Y.; Luan, Z.; Li, Z.; Ji, H.; You, Y. Study on the flow characteristics in the non-detonation reaction zones of wedge-induced oblique detonation transitions. *Aerosp. Sci. Technol.* **2022**, *120*, 107282. [CrossRef]
35. Westbrook, C.K. Chemical kinetics of hydrocarbon oxidation in gaseous detonations. *Combust. Flame* **1982**, *46*, 191–210. [CrossRef]
36. Zhao, H.; Yang, X.; Ju, Y. Kinetic studies of ozone assisted low temperature oxidation of dimethyl ether in a flow reactor using molecular-beam mass spectrometry. *Combust. Flame* **2016**, *173*, 187–194. [CrossRef]
37. Atkins, C.W.C.; Deiterding, R. Modelling Hypersonic Flows in Thermochemical Nonequilibrium Using Adaptive Mesh Refinement. In Proceedings of the 7th European Conference on Computational Fluid Dynamics, Glasgow, UK, 11–15 June 2018; pp. 672–683. Available online: <https://eprints.soton.ac.uk/420989/> (accessed on 2 April 2022).
38. Scoggins, J.B.; Leroy, V.; Bellas-Chatzigeorgis, G.; Dias, B.; Magin, T.E. Mutation++: MULTicomponent Thermodynamic And Transport properties for IONized gases in C++. *SoftwareX* **2020**, *12*, 100575. [CrossRef]
39. Shi, L.; Shen, H.; Zhang, P.; Zhang, D.; Wen, C. Assessment of Vibrational Non-Equilibrium Effect on Detonation Cell Size. *Combust. Sci. Technol.* **2017**, *189*, 841–853. [CrossRef]
40. Choi, J.Y.; Kim, D.W.; Jeung, I.S.; Ma, F.; Yang, V. Cell-like structure of unstable oblique detonation wave from high-resolution numerical simulation. *Proc. Combust. Inst.* **2007**, *31*, 2473–2480. [CrossRef]
41. Verreault, J.; Higgins, A.J.; Stowe, R.A. Formation of transverse waves in oblique detonations. *Proc. Combust. Inst.* **2013**, *34*, 1913–1920. [CrossRef]
42. Browne, S.; Ziegler, J.; Bitter, N.; Schmidt, B.; Lawson, J.; Shepherd, J.E. SDToolbox: Numerical Tools for Shock and Detonation Wave Modeling. In *Technical Report GALCIT Technical Report FM2018.001*; Revised January 2021; Explosion Dynamics Laboratory: Livermore, CA, USA, 2018.
43. Goodwin, D.G.; Speth, R.L.; Moffat, H.K.; Weber, B.W. Cantera: An Object-Oriented Software Toolkit for Chemical Kinetics, Thermodynamics, and Transport Processes. Version 2.5.1. 2021. Available online: <https://www.cantera.org> (accessed on 2 April 2022). [CrossRef]
44. Zhang, Z.; Wen, C.; Yuan, C.; Liu, Y.; Han, G.; Wang, C.; Jiang, Z. An experimental study of formation of stabilized oblique detonation waves in a combustor. *Combust. Flame* **2022**, *237*, 111868. [CrossRef]